



The investigation of the role of basic lanthanum (La) species on the improvement of catalytic activity and stability of HZSM-5 material for eliminating methanethiol-(CH₃SH)



Jichang Lu^a, Husheng Hao^b, Liming Zhang^a, Zhizhi Xu^a, Liping Zhong^a, Yutong Zhao^a, Dedong He^a, Jiangping Liu^a, Dingkai Chen^a, Hongping Pu^a, Sufang He^c, Yongming Luo^{a,*}

^a Faculty of Environmental Science and Engineering, Kunming University of Science and Technology, Kunming, 650500, PR China

^b Environmental Protection Bureau of Wangjiang County, Anqing, 231400, PR China

^c Research Center for Analysis and Measurement, Kunming University of Science and Technology, Kunming, 650093, PR China

ARTICLE INFO

Keywords:

HZSM-5
La modification
Surface active oxygen
Deposited coke
Regeneration

ABSTRACT

Lanthanum (La)-doped HZSM-5 and HZSM-5 catalysts were prepared to investigate the natural roles of La addition on the catalytic performance of HZSM-5 for decomposing methanethiol (CH₃SH). Compared to HZSM-5, the incorporation of La species into HZSM-5 catalyst not only decreased the intrinsic activation energy (from 51.4 kJ/mol to 40.6 kJ/mol) but also largely improved the stability. Based on the characterizations of X-ray diffraction pattern (XRD), N₂ adsorption-desorption, Fourier transform infrared spectroscopy (FTIR), X-ray photoelectron spectroscopy (XPS), temperature-programmed desorption of carbon dioxide (CO₂-TPD), temperature-programmed desorption of ammonia (NH₃-TPD), and temperature programmed desorption of CH₃SH (CH₃SH-TPD), the promotional role of La species on the catalytic activity was demonstrated to be the contribution of the surface active oxygen species within lanthanum oxy-carbonates composites, which not only might act as new active sites for converting CH₃SH into CO₂ but also could decrease the activation temperature for the dehydrogenation of CH₃SH into intermediate, dimethyl sulfide (CH₃SCH₃). The enhanced stability of La doped HZSM-5 was attributed to the synergistic effect of the decrease in the strong acid sites as well as the formed CO₂ and surface lanthanum oxy-carbonates layer. The rapid deactivation of HZSM-5 was due to the formation of deposited coke irrespective of deposited sulfur species. The nature, amount and type of deposited coke were investigated in detail via the characterization of FTIR, Raman spectroscopy, temperature programmed oxidation of oxygen (O₂-TPO), thermogravimetric analysis (TGA). A facile and rapid regeneration method was used to regenerate spent La doped HZSM-5 and no significant deactivation was observed even after three cycles of deactivation-regeneration.

1. Introduction

Photochemical oxidation of volatile organic compounds (VOCs), sulfur species and nitrogen oxides in the atmosphere is primarily responsible for the formation of the severe PM2.5 events, and urban and regional haze pollution in many developing countries [1], especially in China [2]. The removal of organic sulfur compounds together with the reduced sulfur species has attracted considerable attention recently [3,4]. Methyl mercaptan (CH₃SH) is one of typical sulfur-containing VOCs species with very low olfactory threshold (0.4 ppb/v) and extreme toxicity, which is widely produced from many industrial activities and environmental pollution control processes, including energy-related events (e.g., natural gas and oil production), synthesis of DL

methionine, wastewater/sewage disposal and sanitary landfill. More importantly, the emission requirement of CH₃SH is one magnitude lower than that of the most familiar compound, hydrogen sulfide (H₂S), and the indiscriminate emission would cause the more seriously atmospheric pollution issues and the severe poison effects on the human health [1]. Therefore, developing an efficient technique to eliminate CH₃SH is urgently required.

At present, the reported methods for the removal of CH₃SH include catalytic decomposition [5,6], alkaline treatment [7], reaction with olefins [8], hydrodesulfurization [9]. Among them, the catalytic decomposition has been extensively investigated because of its advantages, such as, the easy operation, no need of additional reagents, and the production of a smaller number of contaminants. Therefore,

* Corresponding author.

E-mail address: luoyongming@kmust.edu.cn (Y. Luo).

many researches have focused on the catalytic decomposition of CH₃SH in the past few years [5,6,10,11]. In light of these references, the corresponding catalysts can be basically classified into two types (ZSM-5 and cerium-based oxide catalysts). However, these catalysts generally suffer from the drawbacks of high temperature required for conversion and poor stability (or short lifetime). Huguet and coworkers [10,11] reported that CH₃SH could be selectively transformed into hydrocarbons using pure HZSM-5 zeolite as catalyst. Nonetheless, the corresponding temperature for the complete conversion of CH₃SH was as high as 600 °C. More importantly, the catalyst was deactivated rapidly after no more than 10 h time-on-stream (TOS) test. Compared to HZSM-5, CH₃SH could be completely converted at 450 °C by using nano-scale CeO₂ as the catalyst; however, the fast and significant deactivation was still observed for the catalyst during the stability test (about 8 h TOS test) [12]. Furthermore, in our previous work [5,13], the rare earth (RE) elements modified cerium-based oxide catalysts Ce_{0.75}RE_{0.25}O_{2-δ} (RE = La, Nd, Sm, Y and Gd) were also investigated for the catalytic decomposition of CH₃SH, whereas there was no significant change in the stability of modified cerium-based catalysts. These results indicate that the poor stability of these two type catalysts for CH₃SH decomposition is still not resolved. Importantly, the rapid deactivation mechanism of CH₃SH using these catalysts is not well understood. However, it is well known that the excellent stability of the catalyst is particularly important for its practical applications. Therefore, substantially improving stability and decreasing reaction temperature for the complete decomposition of CH₃SH is a challengeable task [14,15].

HZSM-5 zeolite has recently been used as a catalyst or catalyst support for various catalytic reactions due to its tunable acid-base properties together with well hydrothermal stability [16,17] and is also considered as an alternative material for decomposing CH₃SH [10,18]. It was well documented that the deactivation of HZSM-5-based catalysts for catalytic oxidation of hydrocarbons generally originates from the formation of coke deposit during the reaction due to the presence of strong acidic sites [19,20]. Reducing the strength of acid sites is one of significant strategy for avoiding the deactivation of solid acid catalysts. Since RE oxides usually possess some basic characteristics [21], the introduction of RE elements can effectively tune the acid-base properties of HZSM-5 zeolite, which could reduce the acidity and increase the alkalinity of HZSM-5 zeolite to some degree. More importantly, considering that CH₃SH is an acidic gas, the increasing amounts of basic sites within these RE doped-HZSM-5 samples is believed to be beneficial to the adsorption and activation of CH₃SH molecule. In addition, the production of sulfate was considered to cause the deactivation of catalysts and an acceptable conclusion can be deduced that sulfate compounds will be formed during the interaction between RE oxides over doped catalysts and sulfur species [6]. However, our recent preliminary work on cerium-based catalysts [12] demonstrated that the formation of sulfate species has no influence on the catalytic activity of those materials. These results inspired us to deduce that, during the catalytic decomposition of CH₃SH, the acid-base properties of HZSM-5-based catalysts can be effectively adjusted by the incorporation of RE elements, which will not only improve the catalytic stability to great degree via decreasing the strength of acidic sites but will also significantly enhance the catalytic activity by providing an additional basic center. Compared to other RE elements (Nd and Sm) [14,15], lanthanum (La) oxide possesses unique surface chemical composition and physicochemical property [22]. It is reported that when exposed to air, the top surface of lanthanum oxide was easily subjected to the carbonation and hydroxylation [23,24]. Ramana et al. [23] found that for an air contact time of about 1.5 h, a layer with a thickness of less than 1 nm containing a mixture of lanthanum carbonate and hydroxides can be produced on the catalyst surface under normal conditions by atmospheric agents. The change in the surface chemical composition and structural property of lanthanum oxide makes catalytic reactions (catalytic activity and stability) progressing on the surface of the catalysts more complex. Therefore, investigating the structure-function relations and the

deactivation mechanism in the process of catalytic decomposition CH₃SH by using the La-doped HZSM-5 zeolite as the catalyst is interesting.

In this contribution, two RE elements (Nd and Sm) modified HZSM-5 catalysts were synthesized to compare with La doped HZSM-5 catalyst and the catalytic performances were examined for decomposing CH₃SH. In order to understand the interrelation between the physicochemical properties and catalytic behaviors as well as illustrate the reaction and deactivation mechanisms, XRD, N₂ adsorption-desorption, FTIR, XPS, CO₂-TPD, NH₃-TPD, CH₃SH-TPD, Raman, TGA, and O₂-TPO were employed to characterize these aforementioned catalysts. For industrial application purposes, the catalytic stability together with the regeneration of the spent La/HZSM-5 catalyst were also studied.

2. Experimental

2.1. Catalysts preparation

Commercial HZSM-5 zeolite was obtained from Fuxu Zeolite Company of China, and the corresponding RE nitrates [La(NO₃)₃·6H₂O, Nd(NO₃)₃·6H₂O, and Sm(NO₃)₃·6H₂O] were purchased from Shanghai Chemical Regent Company, China. Commercial HZSM-5 zeolite (calcined at 550 °C in the air for 5 h, denoted as Z-F) was used as the reference as well as the support of RE elements (La, Nd, and Sm) modified HZSM-5 catalysts. These RE-doped HZSM-5 catalysts were prepared by incipient-wetness impregnation method. The calculated amount of RE nitrates was quantitative dissolved in deionized water to keep the 13 wt.% loading of RE (based on La, Nd, and Sm). Next, 5 g of HZSM-5 was added into the above solution under continuous stirring to ensure that all of the liquid was absorbed by HZSM-5. After that, the resulting product was placed at atmospheric temperature for 12 h and then dried at 120 °C for 6 h. Finally, the dried samples were calcined at 550 °C in the air for 5 h, and labeled as La/Z-F, Nd/Z-F, and Sm/Z-F for modification with La, Nd, and Sm, respectively.

2.2. Characterization

XRD patterns of the catalyst samples were recorded using a Rigaku D/max-1200 diffractometer equipped with Cu K α radiation ($\lambda = 1.5406 \text{ \AA}$), operated at 30 mA and 40 kV. The diffraction data were recorded in the 2θ range of between 5 and 50° at a scanning rate of 1° min⁻¹ and a step size of 0.02°. Texture properties were measured by N₂ adsorption-desorption using an automatic adsorption instrument (ASAP 2020) at 77 K. All the samples were outgassed at 523 K in high vacuum (4 mbar) for 2 h before measurement. Specific surface area (S_{BET}) as well as pore size distribution were calculated according to the data of adsorption and desorption branches, respectively. FT-IR measurement was carried using a Nicolet 560 IR spectrometer, and the corresponding spectra of the catalyst samples were recorded in the standard form of KBr pellets at a spectral resolution of 4 cm⁻¹ under atmosphere temperature. XPS was conducted on a PHI 5000 VersaProbe II with non-monochromatic Al K α radiation (1486.6 eV) as the excitation X-ray source to determine the chemical states and surface element compositions of all the catalysts. The charging effect of the catalysts was corrected by referring to the Si 2p_{3/2} peak of SiO₂ (103.3 eV) and the C 1 s peak of adventitious carbon (284.8 eV) [25,26]. The ratio of the surface atoms was calculated by using the peak area ratio normalized by the corresponding atomic sensitivity factor (RSF). Surface acid-base properties of HZSM-5 and La-doped HZSM-5 catalyst samples were characterized by CO₂-TPD and NH₃-TPD, respectively, in which a thermal conductivity detector (TCD) with high sensitivity was employed to continuously monitor the concentration of the desorbed ammonia or carbon dioxide. Prior to NH₃-TPD analysis, 0.2 g of catalyst sample was pretreated with the flow of helium (He, 30 mL/min) at 500 °C for 2 h, and the pretreated sample was cooled down to 100 °C and saturated by using 30 mL/min flow of 10% (v/v) NH₃ within He

under 100 °C for 2 h. Subsequently, the gas mixture was switched back to He and the saturated sample was purged at 100 °C for 1 h to remove the weak and/or physisorbed ammonia (NH_3). Finally, NH_3 -TPD profile of each catalyst sample was recorded by linearly increasing the cell temperature from 100 to 600 °C under the helium flow at 30 mL/min with a heating ramp rate of 10 °C/min. CO_2 -TPD was measured on the same apparatus as used for NH_3 -TPD, and the corresponding procedures of CO_2 -TPD are similar to those of NH_3 -TPD except for the pretreatment of catalyst sample (600 °C), the replacement of NH_3 by CO_2 as well as the adsorption temperature of CO_2 (30 °C).

Spent La doped ZSM-5 and HZSM-5 collected after 40 h TOS test of CH_3SH decomposition, labeled as La/Z-S40 and Z-S40, respectively, were characterized by O_2 -TPO, Raman spectroscopy, XPS, FT-IR and TGA to investigate the effect of deposited coke. O_2 -TPO was performed to investigate the nature and amount of coke deposit as well as its burn-off temperatures. Prior to O_2 -TPO measurement, 0.025 g of sample was pretreated with the flow of helium (He, 30 mL/min) at 500 °C for 1 h for drying and removing volatile compounds and the pretreated catalyst was then cooled down to 100 °C. Subsequently, O_2 -TPO was carried out in the flow of gas mixture (10 v% O_2 within He), and the system was heated from 100 to 800 °C at a ramping rate of 10 °C/min. The onset and degree of coke burn-off were provided via the signal of the measured CO_2 content as a function of temperature. Raman spectra were collected using a Via Reflex Confocal Raman spectrometer in the spectral range of 1000–2000 cm^{-1} , operating at a power of 5 mV with the Ar^+ laser (514 nm) at room temperature. TGA was performed using a TGA Q500 instrument, and the spent samples were heated in the air from atmospheric temperature to 800 °C at a ramp rate of 10 °C/min.

CH_3SH -TPD was performed using a micro-reaction system to further investigate the acid-base properties and the reaction mechanism for decomposing CH_3SH over fresh HZSM-5 and La doped ZSM-5 catalysts. Prior to the analysis, fresh HZSM-5 or La/ZSM-5 was pretreated with air under 550 °C for 1 h and then cooled down to 30 °C. Then, the pretreated sample was adsorbed and saturated with the mixture gas (1 vol % CH_3SH in N_2) at 30 °C for 10 h and subsequently purged with N_2 flow to eliminate physisorbed CH_3SH under 50 °C. Finally, CH_3SH -TPD was performed from 50 to 450 °C in the flow of N_2 at a heating rate of 1 °C/min. The corresponding products were analyzed using two online gas chromatographs (GCs) that were equipped with a thermal conductivity detector (TCD), a flame photometric detector (FPD), and two flame ionization detectors (FIDs) together with a methanation reactor.

2.3. Catalytic activity and stability tests

Catalytic decomposition of CH_3SH was determined in a fixed-bed micro-reactor at atmospheric pressure. In a typical activity test, 0.2 g of catalyst sample with the particle size in the range of 0.25–0.38 mm (60 to 40 mesh) was loaded into a quartz tube reactor. The feed mixture gas containing 10,000 ppm of CH_3SH with the gas flow rate of 30 mL/min was introduced into the catalytic reaction system. 0.4 g of fresh HZSM-5 and La doped HZSM-5 catalysts were used to perform the stability test at 500 °C. The online GC equipped with a FID was used to detect the reactants. The catalytic conversion of CH_3SH was calculated by the following equation:

$$\text{CH}_3\text{SH Conversion} = \frac{C_{[\text{CH}_3\text{SH}]_{\text{in}}} - C_{[\text{CH}_3\text{SH}]_{\text{out}}}}{C_{[\text{CH}_3\text{SH}]_{\text{in}}}} \times 100\%$$

where $C_{[\text{CH}_3\text{SH}]_{\text{in}}}$ represents the initial concentration of CH_3SH before the reaction and $C_{[\text{CH}_3\text{SH}]_{\text{out}}}$ is the remaining ones after the reaction.

According to the integral reactor model and the basic knowledge of kinetics, the kinetic equation was established to estimate the value of the kinetic parameters for decomposing CH_3SH over fresh HZSM-5 and La doped HZSM-5 catalysts, and the apparent reaction rate constant and apparent activation energy were calculated according to the Arrhenius equation:

$$k\tau = \int_0^{X_A} \frac{d\chi_A}{C_{A0}^{n-1}(1-\chi_A)^n}$$

where k is the reaction rate constant, τ is the space time (g·min·mol⁻¹), C_{A0} is the initial concentration of reactant (CH_3SH , mol·L⁻¹), X_A is the conversion of CH_3SH , and n is the reaction order.

In order to obtain intrinsic activation energy, the contribution of diffusional limitations, including internal diffusion and external diffusion, should be eliminated. It is accepted that increasing gas flow velocity is a valid way to eliminate the external mass transfer resistance and decreasing particle size is generally considered to eliminate the internal mass transfer resistance. Therefore, the experimental tests for the conversion of CH_3SH as a function of different gas flow velocities (30, 60, 100, 200, 300, 400, 600 mL/min) with a fixed catalyst size (250–380 μm) and different catalyst size (13–25, 25–75, 75–120, 120–150, 180–250, 250–380, 380–1000 μm) with a fixed flow velocity of 400 mL/min were carried out over HZSM-5 and La doped HZSM-5 catalysts. The external and internal mass transfer resistance were found to be eliminated when the total flow rate was kept constant at 400 mL/min and the catalysts size was 25–75 μm . The intrinsic activation energy of two samples was thus calculated according to the Arrhenius equation.

The turnover frequency (TOF) was used to evaluate the catalytic activity to decompose CH_3SH over fresh Z-F and La/Z-F samples and was calculated by the following equation:

$$\text{TOF} = \frac{F\chi_A}{n_{\text{active sites}}}$$

where F is the reactant flows (mol·s⁻¹), X_A is the conversion of CH_3SH , and $n_{\text{active sites}}$ is the amount of acid sites on the surface (mol).

2.4. Regeneration of spent catalysts

The spent La doped ZSM-5 catalyst was obtained after 110 h TOS test of CH_3SH decomposition under 500 °C. The regeneration of spent La doped HZSM-5 catalyst was carried out by switching the flow of air (30 mL/min) under 500 °C for 1.0 h, and the regeneration temperature is the same as that of TOS test. The regenerated catalyst was directly employed to evaluate its catalytic stability. In order to investigate thermal stability and renewability, La doped HZSM-5 catalyst was carried out for three cycles of deactivation and regeneration, denoted as La/Z-R1, La/Z-R2, and La/Z-R3.

3. Results and discussion

3.1. Catalytic activity

CH_3SH conversions at different temperature of 400 °C and 450 °C over Z-F, La/Z-F, Nd/Z-F, and Sm/Z-F catalysts are shown in Fig. 1(A) and (B), respectively. In order to confirm the effect of the reaction temperature on the ability to decompose CH_3SH , the CH_3SH conversion of the blank sample at the different reaction temperatures is also displayed in Fig. 1A (a) and B (a). The corresponding conversion of CH_3SH is lower than 5% at 400 and 450 °C, and rising the reaction temperature slightly increases the conversion of CH_3SH , demonstrating the weak ability for the decomposition of CH_3SH without the addition of catalysts. When the catalyst samples are added into the reaction system, as displayed in Fig. 1A, Z-F sample exhibits the relatively high CH_3SH conversion (67%) at 400 °C, proving the enhanced catalytic ability for decomposing CH_3SH over HZSM-5 zeolites. At this temperature, the addition of REs (La, Nd, and Sm) into HZSM-5 sample slightly improves the decomposition of CH_3SH . With further increasing reaction temperature to 450 °C (Fig. 1B), parent HZSM-5 sample shows the same CH_3SH conversion with that at 400 °C, whereas significant improvement in the conversion of CH_3SH is observed with the addition of La, Nd, and Sm into HZSM-5 catalyst. The modification of La, Nd, and Sm

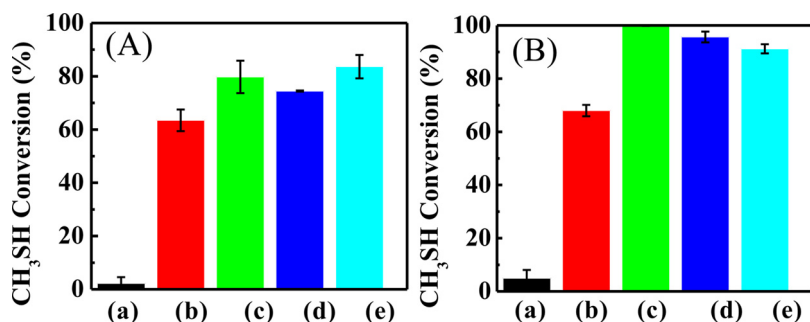


Fig. 1. CH₃SH conversion of HZSM-5 and rare earth (La, Nd and Sm) modified HZSM-5 catalysts under (A) 400 °C and (B) 450 °C. (a) blank without catalyst, (b) Z-F, (c) La/Z-F, (d) Nd/Z-F, (e) Sm/Z-F.

Table 1

Estimated values for kinetic parameters of Z-F and La/Z-F catalysts.

Catalysts	k ($L^2 \cdot mol^{-1} \cdot g^{-1} \cdot min^{-1}$)	E_A^1 (kJ/mol)	E_T^2 (kJ/mol)	TOF ($\times 10^{-3}$ s $^{-1}$)
				450 °C
Z-F	102	32.4 ± 0.4	51.4 ± 1.4	1.56
La/Z-F	232	24.2 ± 0.3	40.6 ± 1.2	3.24

¹ apparent activation energy.

² true activation energy.

into HZSM-5 significantly increases the CH₃SH conversion from 68% to 100%, 95% and 91%, respectively, indicating that REs play a significant role in the elimination of CH₃SH. Among them, La is found as the optimal RE element for improving the catalytic activity of CH₃SH decomposition, which reduces the reaction temperature of full conversion to 450 °C. The corresponding reaction rate constant at 450 °C, reaction activation energy, and TOF values over Z-F and La/Z-F samples for decomposing CH₃SH are listed in Table 1. It is shown that the apparent reaction rate constant is larger for La/Z-F sample (232 L²·mol⁻¹·g⁻¹·min⁻¹) than that for Z-F sample (102 L²·mol⁻¹·g⁻¹·min⁻¹), consistent with activity result. The addition of La species decreases the intrinsic (apparent) activation energy for decomposing CH₃SH from 51.4 kJ/mol (32.4 kJ/mol) to 40.6 kJ/mol (24.2 kJ/mol). Meanwhile, TOF exhibits the higher value of 3.24×10^{-3} s⁻¹ for La doped HZSM-5 sample than that of 1.56×10^{-3} s⁻¹ for HZSM-5 sample. All these results indicate that the incorporation of La species largely improves the catalytic activity to decompose CH₃SH. La-doped HZSM-5 and HZSM-5 samples were thus selected to thoroughly investigate the reason in the activity difference among parent HZSM-5 zeolite and REs modified HZSM-5 samples.

3.2. Characterization of the crystalline structure and the chemical state of La species

After the addition of La species into HZSM-5 sample, the textural and the structural properties of HZSM-5 sample possibly change. A series of characterization, including N₂ adsorption-desorption isotherms, FT-IR, XRD, and XPS, are used to investigate the role of La additive on the properties of parent HZSM-5. N₂ adsorption-desorption isotherm of La/Z-F sample is compared to that of Z-F as shown in Fig. 2(A), and the corresponding textural parameters are summarized in Table 2. Based on the IUPAC classification, N₂ adsorption-desorption isotherm of La/Z-F is found to be of type I, which is very similar to those of parent HZSM-5 and an indication of typical microporous structure. There is no significant change in the uptake of nitrogen (N₂) at a relative pressure (P/P₀) in the range of 0.1–0.9, arising from the capillary condensation within mesopores via nitrogen multilayers adsorbed on the inner surface [27,28]. In addition, a small N₂ uptake step at P/P₀ > 0.9 is observed for both Z-F and La/Z-F samples, characteristics of interparticle macroporosity [29,30]. As listed in Table 2, with the

addition of La, BET micropore surface areas and pore volumes decrease accompanied by the increase in the external surface area, probably suggesting that partial La species enter into the micropore channel and substitute with the Al species, and additional Al-OH species generate on the external surface of HZSM-5 due to the dealumination, which is confirmed by the following FTIR spectra.

FT-IR spectra of the catalyst samples are carried out to further confirm the dealumination, the OH-stretching vibrations are generally characterized in the range of 3000–3800 cm⁻¹ over Z-F and La/Z-F samples, and the corresponding result is shown in Fig. 2(B). Two important bands are observed between Z-F and La/Z-F samples. The first one is the well known band at 3610 cm⁻¹, which is assigned to the O–H stretch vibrations originated from bridging Si-(OH)-Al groups within the zeolite framework, generally regarded as the Brønsted acid sites [31,32,33]. This bridging OH species inside zeolite framework is obviously observed for parent ZSM-5 sample, while it disappears with the addition of La species into HZSM-5 catalyst, indicating that those Brønsted acid sites are possibly occupied by the addition of La species. Furthermore, the second band is found to be located at 3660 cm⁻¹, which is attributed to the OH groups related to extra-framework aluminum species [34,35]. The intensity of this band largely increases with La species doped. The change in these two bands (at 3610 and 3660 cm⁻¹) is of great interest and seems to imply that Al-OH species from the bridging Si-(OH)-Al groups in the zeolite framework structure are possibly substituted by partial La species in the preparation process and released from the ZSM-5 zeolite framework to form new external Al-OH groups (dealumination). Furthermore, the small and broad region in the range of 3610–3635 cm⁻¹ is visible for La/Z-F and should be correspond to the hydroxyls attached to La ions [33,36,37], implying the possibility of the replacement of Al-OH by La-OH species. In the literature, this decrease in the intensity of the band at 3610 cm⁻¹ has been previously reported by Topsoe et. al. to regard as an informative way for dealumination [38]. Othman et. al. and Villegas et. al. also have observed the dealumination phenomenon over La modified ZSM-5 on the decolorization of indigo carmine dye and Pt-modified mordenite zeolite on the isomerization of n-butane, prepared by the impregnation method [39,40]. This phenomenon can be further confirmed by calculating the Si/Al ratio via the characterization of XPS (not shown). The ratio of Si/Al is calculated to be 28.1 for parent ZSM-5, while the corresponding ratio decreases to 22.5 after the incorporation of La species, evidencing the increase in the external aluminum species. The occurrence of the framework dealumination probably leads to the aggregation of partial La-OH species into La oxide clusters during the high temperature calcination. The decrease in the number of strong Brønsted acid sites via dealumination accompanied by forming an extra framework aluminum plays an important role in limiting the generation of coke to some degree. In addition, another band at 3746 cm⁻¹ characteristic of silanol groups [32,41] should be strong and main components in typical ZSM-5 zeolite. However, only low and small intensity of silanol groups are observed, even, for parent ZSM-5 sample. This is probably likely to be related to the condensation of surface silanol

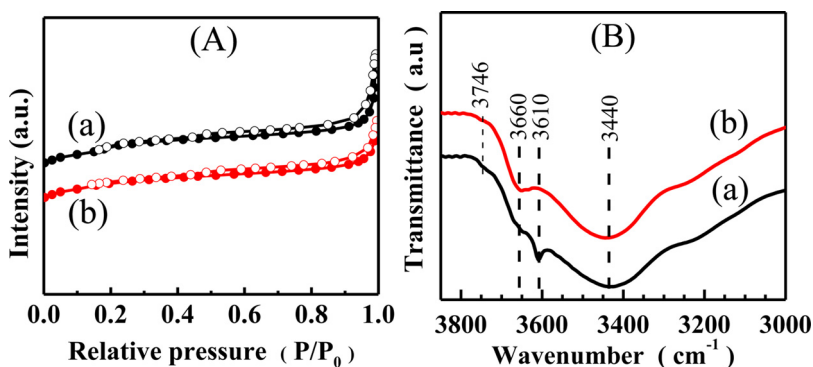


Fig. 2. N₂ adsorption-desorption isotherms (A) and FT-IR spectra in the region of 3000–3800 cm⁻¹ (B) of fresh samples: (a) Z-F, (b) La/Z-F. The isotherm of (b) is offset by 140 cm³/g for clarity.

Table 2

Textural properties as well as surface acidity and basicity of Z-F and La/Z-F catalysts.

Catalyst	S _{BET} (m ² / g)	S _{micro} (m ² / g)	S extern (m ² / g)	Pore volume (cm ³ /g)	Acidity (umol/g) ^a		Basicity (umol/g) ^a
					Weak	Strong	
Z-F	402.6	379.5	23.1	0.269	474.44	234.87	5.02
La/Z-F	314.2	287.0	27.2	0.201	343.94	106.41	22.34

S_{BET}: BET surface area was calculated by using Brumauer-Emmett-Teller (BET) mode.

S_{micro}: micropore area was determined from t-Plot micropore area.

S_{extern}: external surface area was determined from t-Plot micropore area.

Pore volume: single point adsorption total pore volume.

^a Determined by quantifying the desorption peak area of defined molecules (NH₃ and CO₂, respectively) from NH₃/CO₂-TPD profiles.

groups in parent ZSM-5 sample. The formation of Si-O-Si groups is confirmed by a big band at 801 cm⁻¹ [42].

The crystalline structural features of Z-F and La/Z-F catalysts are displayed in the XRD patterns of Fig. 3(A). The typical diffraction peaks of mordenite framework inverted (MFI) structure [43] centered in the 2θ ranges of 7–9° and 23–25° are detected for all the catalyst samples, suggesting that the zeolitic characteristics of La-doped HZSM-5 catalyst samples is maintained without any structural change. Moreover, three new small and broad diffraction peaks centered at 2θ = 28.1°, 39.4° and 49.0° are well observed in the XRD pattern of La/Z-F in comparison to those of parent Z-F sample. When compared to the power diffraction standard from JCPDS database, the locations of three strongest diffraction lines are found to be close to three other La species, La₂O₃ species (PDF#40-1284), La₂O(CO₃)₂ (PDF#32-0490) and La₂O₂CO₃ (PDF#48-1113), because of their similar crystalline structure. The presence of this broad and small X-ray diffraction signal of La species in La/Z-F might be due to the existence of La species in the form of

oligomerized species (dimer, cluster, etc.) or to the presence of La species with small size or amorphous structure. However, it is difficult to prove whether all three La containing species are presented via the characterization of XRD technique.

The structural information of Z-F and La/Z-F catalysts are further characterized by FTIR in the range 400–2000 cm⁻¹, as shown in Fig. 3B. As seen, the bands centered at 801 and 1225 cm⁻¹ are ascribed to the vibrations associated with external connections between tetrahedral [44,45] and are documented as the structure-sensitive IR bands of ZSM-5 zeolite [46,47]. Two bands at about 454 and 1100 cm⁻¹ observed in the spectra of parent Z-F and La/Z-F catalysts are attributed to the internal five-membered ring O-T-O asymmetric vibration relating with the SiO₄ and AlO₄ tetrahedral within ZSM-5, respectively [48]. Another band located at 553 cm⁻¹ was assigned to external double ring vibration of ZSM-5 zeolite (five-membered ring subunits) [14,47]. Those bands are representative of typical ZSM-5 zeolite and suggest that the incorporation of La species into HZSM-5 zeolite does not alter the entire framework structure of HZSM-5 zeolite. The usage of the intensity ratio of the peak in the range from 553 cm⁻¹ to 454 cm⁻¹ as a criterion for determining the crystallinity of ZSM-5 zeolite was demonstrated to be efficient [48]. The corresponding percentage of crystallinity for Z-F and La/Z-F samples are calculated to be 78.7% and 70.5%, respectively. The decrease in the crystallinity over La/Z-F samples suggests that most La species are possibly presented in the form of clusters with small size inside the ZSM-5 pore channel [48,49]. Notably, the infrared spectrum of La/Z-F shows weak bands at 1520 and 1470 cm⁻¹ associated with the structures of La₂O_x(CO₃)_y species [24,50,1]. La oxide clusters in the La/Z-F sample seem to consist of complex La₂O_x(CO₃)_y species. The presence of this phase was further confirmed by XPS characterization.

The chemical component and elemental valence state of La oxide species are further characterized by XPS. The XPS spectra of Z-F and La/Z-F samples in the La 3p, C1s and O 1s region are displayed in the Fig. 4. Since the interaction of spin-orbit coupling, the signal of La 3d

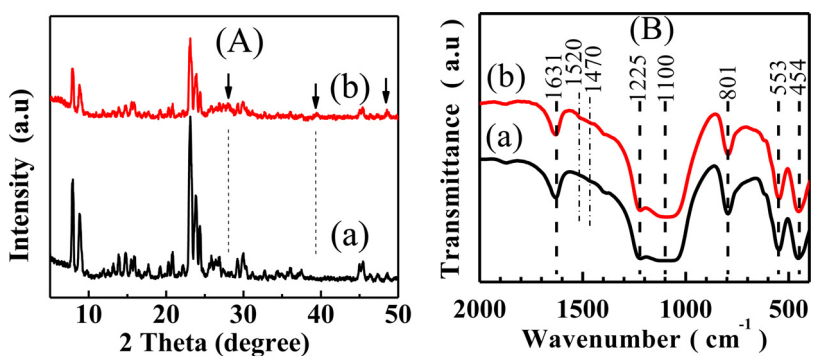


Fig. 3. XRD patterns (A) and FT-IR spectra in the region of 400–2000 cm⁻¹ (B) of fresh samples: (a) Z-F, (b) La/Z-F.

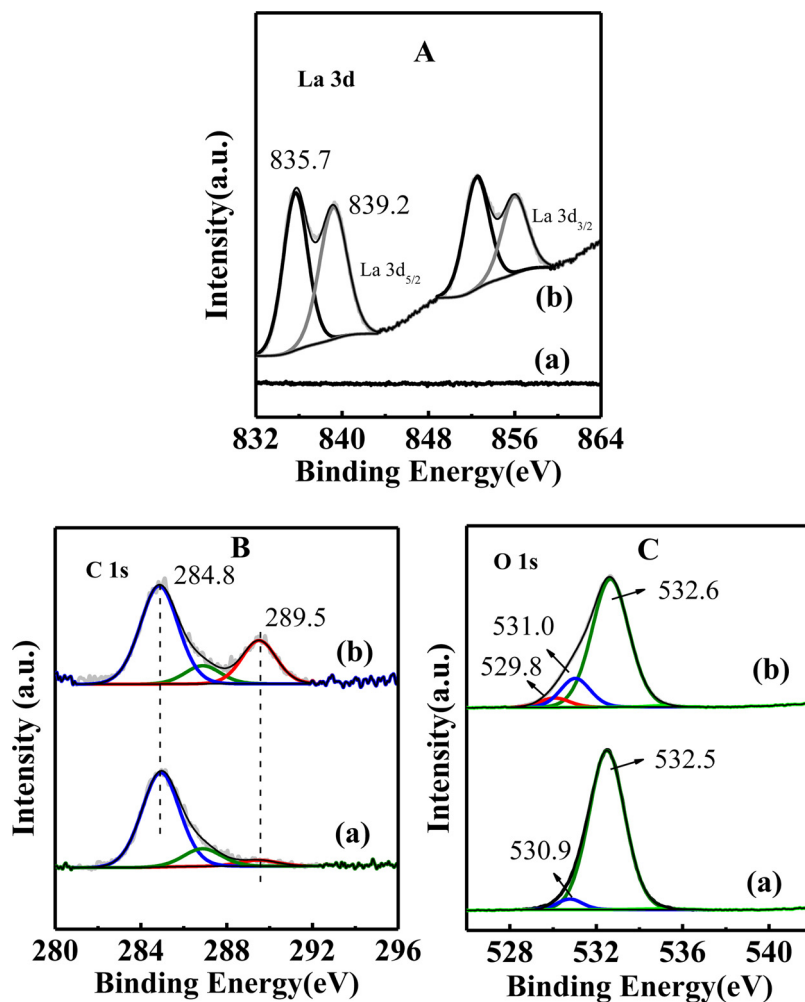


Fig. 4. XPS spectra of La 3d (A), C 1 s (B) and O 1 s (C) for the fresh samples: (a) Z-F, (b) La/Z-F.

electrons in the region of 832–860 eV is split into the 5/2 and 3/2 components. Those La 3d_{5/2} and La 3d_{3/2} peaks are found to be doublets with a small energy difference, suggesting that La species is presented in the form of two different bonding states with a great extent of mixing [51]. For the La 3d_{5/2} region, the oxidation state of La species is generally considered to be +3 due to the observed binding energy at 835.7 eV. However, this binding energy is greatly higher than those reported for the La 3d_{5/2} binding energy in La₂O₃ and supported La₂O₃ (833.2–834.8 eV) [23,52]. This phenomenon of the large shift to higher binding energy (1 eV) has been observed for Cu 2p in Cu/ZSM-5 [53] and O1 s in type ABO₃ perovskite [54], and seems to be related with the decrease in the electron density, because of the change in the coordination mode and surrounding environment in corresponding species. This increased binding energy of Cu and O species had been attributed to the presence of isolated metal ions/small clusters of ions and oxygen ions with low coordinate state at the catalyst surface, respectively. Indeed, higher binding energy in the range of 835.0–835.5 eV was also reported [23,37] and assigned to La³⁺ being connecting with carbonates or La oxide being bonding with carbonates (La₂O_x(CO₃)_y). Since La species is presented on the catalyst surface as low-coordinated clusters of La₂O₃ with surface La₂O_x(CO₃)_y ($0 \leq x,y \geq 3$) layer, the binding energy of La species is thus higher than that of the conventional value of La₂O₃. The presence of the corresponding carbonates and oxygen species in the La₂O_x(CO₃)_y are further proved by the C 1 s and O 1 s spectra of Z-F and La/Z-F samples and the results are shown in Fig. 4(B) and (C), respectively. Even though pure Z-F shows the presence of small absorbed carbonates species at 289.5 eV, the large C 1 s

peak at 289.5 eV is obviously observed for La/Z-F and should be ascribed to the carbon in the form of carbonates interacting with La₂O₃ species [55]. The asymmetric O1 s peak of the La/Z-F catalyst exhibits the existence of different types of oxygen species. The low binding energy at 529.8 eV is only observed for La/Z-F catalyst. Compared to typical BE of bulk and surface lattice oxygen in bulk La₂O₃ and other metal oxides within the range of 528.1–529.0 eV and 529.0–529.5 eV, respectively [23,54], this binding energy shift of oxygen peak to higher position indicates that this species is in the low coordinate state with La³⁺ ion and is related to the surface lattice oxygen species bonding to La³⁺ ion with low electron density [56]. The second component at 531.0 eV is typically assigned to oxygen species for both carbonate (CO₃²⁻) and hydroxyl (OH) species [55,56]. The obtained XPS information of the La, C, and O species within outer 2–5 nm of the solid demonstrates the formation of La₂O_x(CO₃)_y ($0 \leq x,y \geq 3$) species on the surface of La₂O₃ species [57]. To confirm the presence of all the La₂O₂CO₃ and La₂O(CO₃)₂ species on the catalyst surface, the corresponding content ratio of oxygen at 531.0 eV to surface lattice oxygen at 529.8 eV is compared and found to be 3.1, between the value of 1.5 and 6 for La₂O₂CO₃ and La₂O(CO₃)₂ species, respectively. This result indicates that the interaction of partial La₂O₃ with CO₂ in the air leads to the generation of carbonated lanthanum oxycarbonates, both La₂O₂CO₃ and La₂O(CO₃)₂ species. It is important to note that basic lanthanum oxides easily suffer from the carbonation and hydroxylation that can progress into bulk to a different degree depending on the material [24]. The XPS observation of a-La₂O₃ films reported by Ramaña et al. demonstrated that a layer with a thickness of < 1 nm of

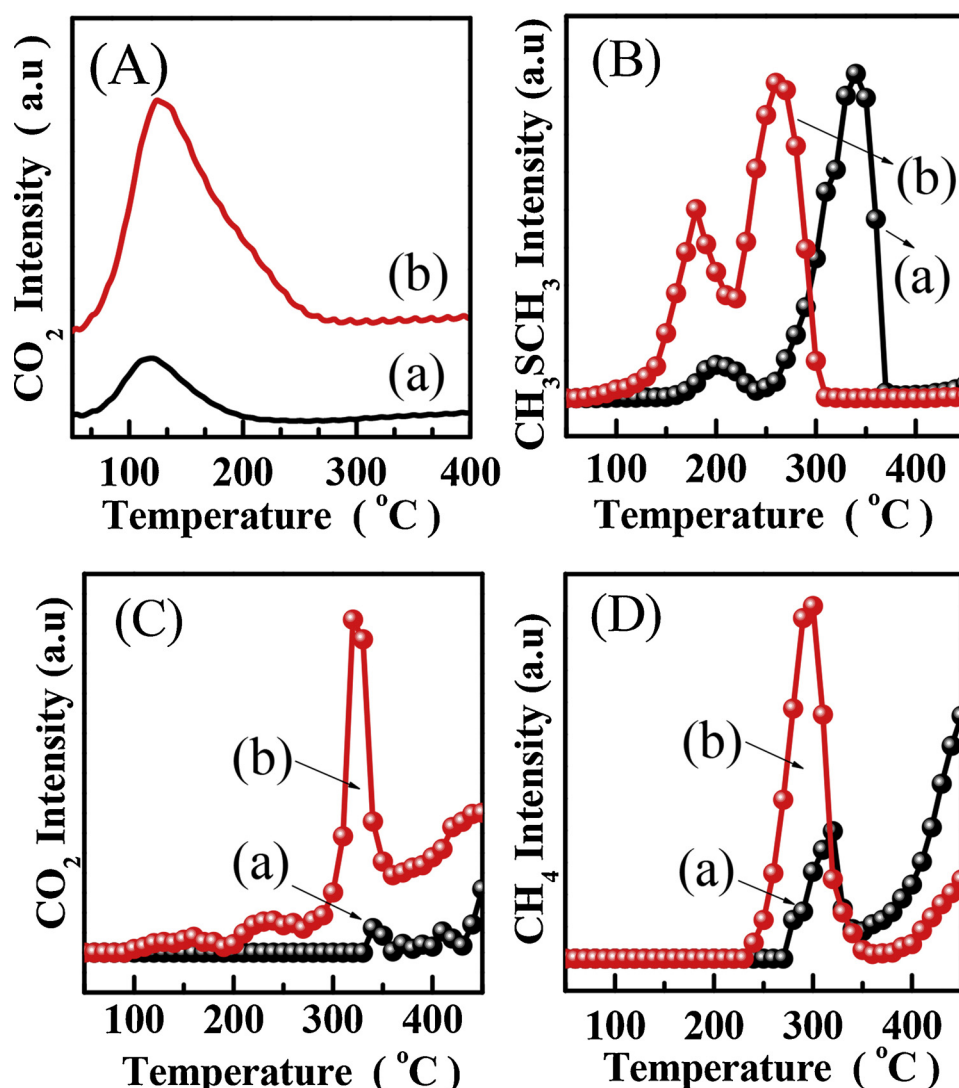


Fig. 5. (A) CO₂-TPD profile of fresh samples: (a) Z-F and (b) La/Z-F. (B) CH₃SCH₃, (C) CO₂ and (D) CH₄ signal during the course of CH₃SH-TPD over Z-F (a) and La/Z-F (b).

lanthanum hydrocarbonates may be formed at an air contact time of about 1.5 h [23]. Therefore, this unexpected lanthanum oxy-carbonates might be inevitably generated on the surface of any La oxide containing materials during the calcination when exposed to the air or during the reaction of CO₂ and can be deemed to be a stabilized catalytic component to participate in the whole catalytic process. Moreover, the higher binding energy at about 532.5 eV observed for both Z-F and La/Z-F samples are corresponding to the surface oxygen of typical Si-O-Si originating from the condensed silanol groups, as detected in the FTIR spectra.

3.3. Possible mechanisms for the enhanced activity

It is initially deduced from above results that the formed La₂O₃ clusters as well as surface lanthanum oxy-carbonates are responsible for the enhanced catalytic activity. Those La oxide species are generally regarded as the basic sites due to their intrinsic basic characteristics. Thus, CO₂-TPD is used to characterize the basicity of Z-F and La/Z-F samples, and the corresponding profiles and the amount of basic sites are shown in Fig. 5(A) and Table 2, respectively. Fig. 5(A) shows a small CO₂ desorption peak at 117 °C for Z-F catalyst, indicating the existence of a small amount of basic sites for parent HZSM-5 sample (5.02 μmol/g). La/Z-F sample shows an increased and asymmetric CO₂ desorption

peak suggesting that the amount of basic sites significantly enhances (22.34 μmol/g) and new basic sites form upon the incorporation of La species. The slight shift of corresponding desorption temperature to high position (125 °C) also indicates the increase in the strength of basicity of La/Z-F sample. Since CH₃SH molecule is strongly acidic, the increase in the amount and strength of basic sites as well as the creation of new basic sites for La/Z-F catalyst will be in favor of the adsorption or reaction of more CH₃SH molecules [13,14]. To deeply investigate the insight roles of basic sites via the La addition for enhancing the catalytic activity during the catalytic decomposition of CH₃SH, Z-F and La/Z-F samples are characterized by CH₃SH-TPD, and the corresponding results are presented in Fig. 5B-D. In addition to the desorbed reactant CH₃SH (not shown), three main desorbed products, dimethyl sulfide (CH₃SCH₃, DMS), carbon dioxide (CO₂) and methane (CH₄), are detected. DMS is known as one of important intermediates generated via the dehydrogenation of two CH₃SH molecules during the decomposition of CH₃SH over ZSM-5 catalyst and the decomposition of DMS ultimately forms products such as methane, hydrogen sulfide and other carbon-containing matters [10,11], as confirmed by the detected DMS and CH₄ in Z-F and La/Z-F samples (Fig. 5B and D, respectively). As displayed in Fig. 5B, the main desorption peak of CH₃SCH₃ over Z-F sample is located at 340 °C accompanied by a shoulder desorption peaks at 200 °C, which is in good agreement with the generated temperature

of DMS between 300 and 400 °C [10,11]. However, with the addition of La species, the main and shoulder desorption peaks in La/Z-F sample significantly shift to the lower temperature (259 °C and 180 °C) followed by the increased desorption area of the shoulder peak. This result combined with the results of CO₂-TPD indicates that more basic sites were generated within La/Z-F sample, and the basic sites might play a significant role in decreasing the activation temperature of the first step reaction of the dehydrogenation to generate DMS species. The generated basic characteristic by the addition of La species might provide new active sites, which can facilitate the process of adsorption, activation, and desorption of CH₃SH molecule and generate more intermediates during the catalytic reaction. This observation provides a direct proof that the outstanding enhancement of catalytic activity for decomposing CH₃SH over La/Z-F catalyst at low temperature region is related to the activation of CH₃SH molecule to intermediate DMS via the modification of La species.

Another important insight of La species on the enhanced catalytic activity is provided by the desorbed CO₂ peak during the course of CH₃SH-TPD. As shown in Fig. 5C, CO₂ desorption peak is not observed in parent Z-F sample, while a great number of CO₂ peak is detected in the desorbed products of La/Z-F sample. In the parent Z-F sample, all the oxygen species, originating from the Si-O-Si groups and small absorbed CO₃²⁻ and OH⁻ species (detected by XPS in Fig. 4C), are generally considered to be inactive with carbon containing molecules, hence leading to the production of trace amounts of CO₂. However, for La/Z-F sample, with the addition of La oxide species, some surface lattice oxygen and surface carbonated oxygen from detected outlayer (La₂O_x(CO₃)_y) species are generated. Thus, those reactive and readily available oxygen species could react with C containing species in the intermediate (DMS) and/or reactant (CH₃SH), generating large amount of CO₂, due to the carbocation chemistry on the acid sites [58]. Our recent study of Ce_{1-x}Y_xO₂-δ for decomposing CH₃SH was proved by using a series of designed experiments and characterization by TPR and XPS that surface lattice oxygen were responsible for decomposing CH₃SH [59]. Therefore, it is speculated that the basic sites (i.e., readily available reactive oxygen species) derived from La oxide as well as surface lanthanum oxy-carbonates species could act as an additional active sites in La/Z-F to react with carbon containing molecules to produce CO₂. The occurrence of this reaction also decreases the reaction temperature and improves the catalytic activity.

3.4. Catalyst stability and deactivation mechanism

The stability of the catalyst is of utmost importance for its practical application [15,60,61]. Therefore, the TOS experiment was carried out under the actual reaction conditions to investigate and compare the catalytic stability of Z-F, La/Z-F, Nd/Z-F, and Sm/Z-F catalysts, and the corresponding results are displayed in Fig. 6. As shown, the CH₃SH conversion using Z-F catalyst decreases to zero after 40 h, while that using La/Z-F sample maintains at 95% in the first 90 h, which is nearly five times longer than those of Z-F sample and is longer than that of Nd/Z-F and Sm/Z-F samples, thus indicating the tremendous improvement in the catalytic stability of CH₃SH decomposition due to the addition of La species.

In the process of eliminating sulfur and carbon containing contaminants for HZSM-5 type materials, the deactivation caused by the deposition of sulfur and carbon species can not be avoided. In the process of typical hydrodesulfurization, the deactivation by sulfur poisoning was almost universal, and thus sulfided Co(Ni)Mo(W)S₂ materials were usually used as the catalysts to void the poisoning by sulfur containing species. However, it is not known that whether Z-F and La/Z-F catalysts are easily poisoned by sulfur or not when used for the decomposition of CH₃SH. In order to further investigate and confirm the mechanism of deactivation, La/Z-F sample after 110 h of stability test was regenerated in air at 500 °C for 1.0 h, and the stability test of the regenerated La doped ZSM-5 sample was performed under

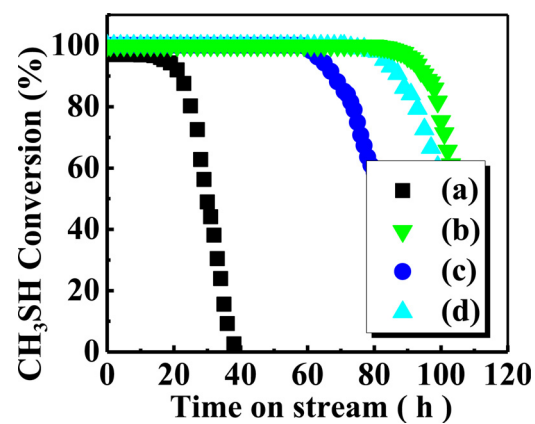


Fig. 6. The stability test for conversion of CH₃SH as a function of time on stream at 500 °C over fresh samples: (a) Z-F, (b) La/Z-F, (c) Nd/Z-F and (d) Sm/Z-F.

the same conditions. The corresponding sulfur species of Z-F, La/Z-F, Z-S40, La/Z-S40, and La/Z-R1 are characterized by XPS, and their XPS S 2p spectra are shown in Fig. 7(A). Fresh Z-F and La/Z-F samples did not show any signal of sulfur species, whereas the S 2p_{3/2} peak at 164.0 eV, between 161.4 eV (S²⁻) and 169.4 eV (S⁶⁺), is observed for Z-S40 sample (Fig. 7A (b)), indicating the formation of the sulfur species with the valence state in the range from -2 to 6+. According to the relevant data, this binding energy is associated with the presence of elemental sulfur (S°) [62,63], possibly originated from the breaking of the C–S bond in CH₃SCH₃ or CH₃SH molecules on the acid sites during the decomposition of CH₃SH. As for La/Z-S40 sample, in addition to the peak corresponding to elemental sulfur, additional S²⁻ species is detected at the binding energy of 161.4 eV [64]. It is found that the relative content of sulfur species (S° and S²⁻) is higher for La/Z-S40 (Fig. 7A (d)) than that for Z-S40 (Fig. 7A (b)). However, La/Z-S40 catalyst still shows the 100% conversion, while the conversion of Z-S40 catalyst decreases to zero. Thus, those sulfur species (S° and S²⁻) are not the factor inducing the deactivation of catalysts. After the regeneration of La/Z-F sample, large amount of other sulfur species, SO₄²⁻, at 169.4 eV is also detected due to the reaction of sulfur species (S° and S²⁻) with oxygen in the air (Fig. 7A (e)). Nevertheless, La/Z-R1 catalyst still exhibits 100% conversion (Fig. 10), indicating that all the sulfur species (S°, S²⁻ and SO₄²⁻) are not the major factor deactivating the catalysts, and they are neither likely to deposit on the active sites nor to block the pore channel of ZSM-5 type catalysts in the composition of CH₃SH. Therefore, it is speculated that the coke deposited might play a large role in determining the deactivation of catalysts.

O₂-TPO, TGA, Raman spectroscopy, and FTIR techniques are used to investigate the nature, amount, and type of coke deposited over Z-S40 and La/Z-S40 catalysts during the catalytic decomposition of CH₃SH. The nature of coke deposited during the decomposition of CH₃SH is analyzed by O₂-TPO. The O₂-TPO profiles of Z-S40 and La/Z-S40 samples are displayed in Fig. 7(B). Only one big peak at 570 °C is obtained for Z-S40 sample, which is an evidence of a homogeneous coke corresponding to a condensed composition of coke with a low H/C ratio [65,66]. The low temperature region in the range of 180–300 °C might be assigned to the slightly developed coke with more reactive to oxygen [66]. After the incorporation of La into HZSM-5, the combustion peak of coke shifts to lower temperature (553 °C). The slight decline in the temperature of oxidation peak indicates that La/Z-S40 sample possesses the enhanced coke burn-off performance. Furthermore, the peak area of La/Z-S40 sample is found to be far smaller than that of parent Z-S40 sample, suggesting that less coke deposit was oxidized over La/Z-S40 sample in the process of O₂-TPO. The amount of coke deposited over Z-S40 and La/Z-S40 samples could be determined by TGA and the result is displayed in Fig. 7(C). The TGA curve suggests that the high

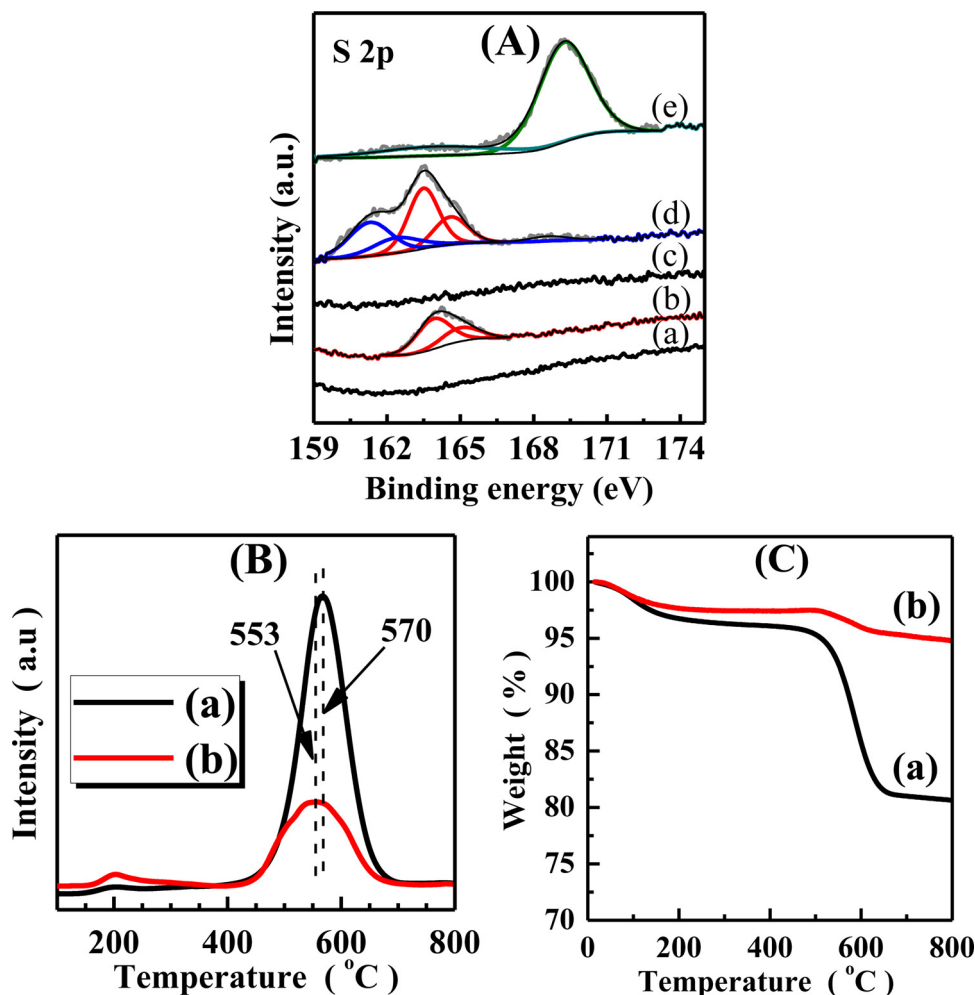


Fig. 7. (A) Decomposition of XPS S 2p spectra of the catalytic systems: (a) Z-F, (b) Z-S40, (c) La/Z-F, (d) La/Z-S40 and (e) La/Z-R1. (B) O₂-TPO profiles, (C) weight loss as function of temperature of (a) Z-S40, (b) La/Z-S40.

temperature weight loss between 500 and 650 °C is due to the combustion of deposited coke. In addition, the corresponding coke content of Z-S40 and La/Z-S40 samples was found to be about 15.38 and 2.59 wt%, respectively, indicating the significant decrease of the deposited coke with the addition of La species. It is known that the formation of deposited coke could give rise to the deactivation via protecting the reactant molecules from entering the active sites or directly covering the acidic reactive center. Compared to the maximum content that can be deposited inside the micropores of ZSM-5 zeolite (about 11–12 wt.% for a standard ZSM-5 sample), for HZSM-5 sample, it seems to consider that a large number of coke was accumulated inside parent ZSM-5 channel blocking the micropores. Although a certain fraction of coke deposited on La doped ZSM-5, the catalytic activity maintains 100%, which implies that partially deposited coke is possibly eliminated and enough number of active centers can be utilized to react with reactant molecules, CH₃SH.

To further obtain the detailed type of coke components, two vibration regions in the infrared spectrum of deposited coke in the ranges of 1300–1700 cm⁻¹ and 2700–3100 cm⁻¹ are provided in Fig. 8(A) and (B), respectively. According to the literature classification, the first regions between 1300–1700 cm⁻¹ is mainly characteristic of unsaturated coke components (polyolefins and condensed aromatics) and bending vibrations of aliphatics, and the second region between 2700–3100 cm⁻¹ is generally associated with the stretching vibrations of aliphatics (paraffins and olefins) [58,65,67]. Respectively, the big and broad band is observed in the region of 1550–1700 cm⁻¹ for both Z-

S40 and La/Z-S40 samples, suggesting the presence of different types of coke species. Among them, the first band at 1620 cm⁻¹ is assigned to the C=C stretching vibration of a complex mixture of unsaturated hydrocarbons, i.e., polyolefins [67,68]. Two bands at 1598 and 1580 cm⁻¹ are due to the C=C bending vibration of polycondensed aromatics species, namely coke [65,68]. The presence of larger intensity bands of Z-S40 than that of La/Z-S40 sample indicates that the addition of La species decreases the formation of coke in the form of polyolefins and polycondensed aromatic species. Furthermore, some low frequency bands at 1379, 1450, and 1465 cm⁻¹ ascribed to the C–H bending vibration of –CH₃ (symmetric), –CH₂ or –CH₃ groups (asymmetric), in-plane bending vibration of –CH₂ [65,69], respectively, and the high frequency bands at 2854, 2927, and 2962 cm⁻¹ corresponding to the C–H stretching vibration of –CH₂ (symmetric), –CH and –CH₂ (asymmetric), and –CH₃ groups (asymmetric) [68], respectively, are obviously observed for HZSM-5 sample, demonstrating the existence of a large number of branched aliphatics on this catalyst after 40 h TOS. For La/Z-S40 sample, however, the intensity of both low frequency and high frequency bands significantly decrease, suggesting that the incorporation of La species largely reduces the generation of coke in the form of branched aliphatics. Notably, the band at 1640 cm⁻¹ over Z-F and La/Z-F samples are assigned to the moisture in the zeolite samples. Thus, water present as the moisture could give rise to some adsorption at 1640 cm⁻¹ for spent Z-S40 and La/Z-S40 samples, which might affect the amount of deposited carbonaceous species to some extent, i.e., polyolefins. Thus, Raman spectroscopy was further used to confirm the

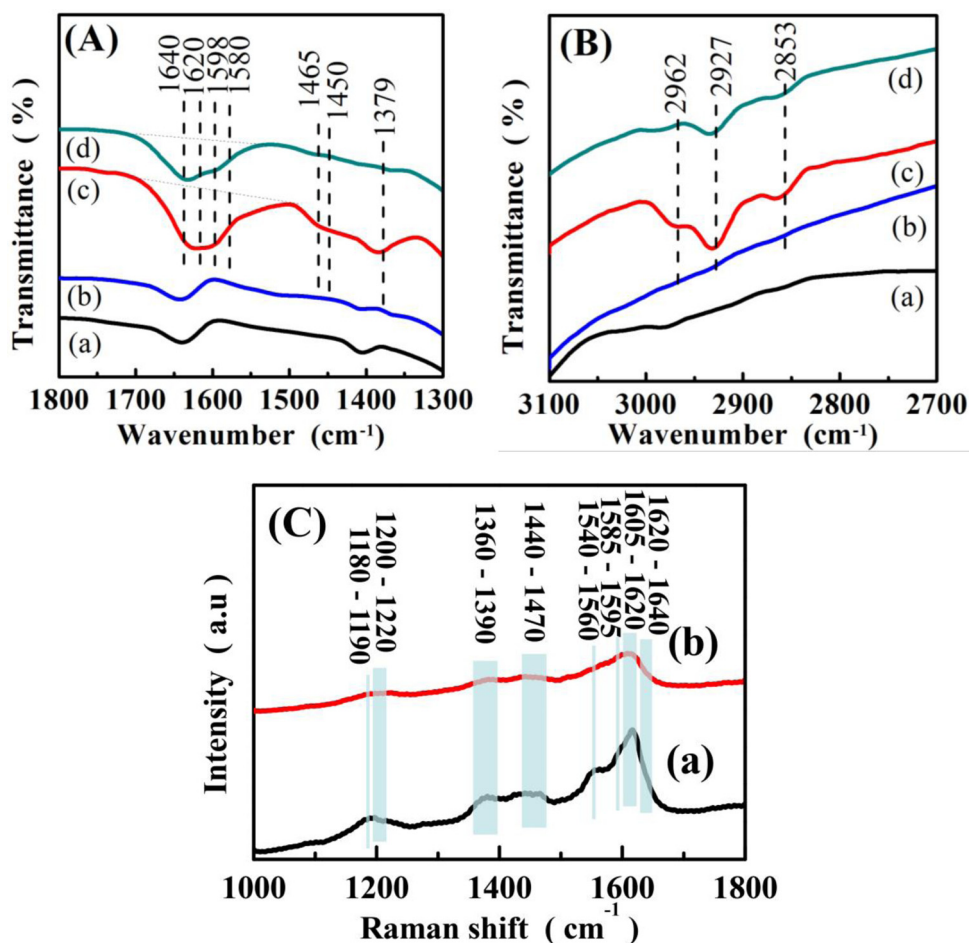


Fig. 8. FT-IR spectra in the region of 1300–1800 cm⁻¹ (A) and 2700–3100 cm⁻¹ (B) of (a) Z-F, (b) La/Z-F, (c) Z-S40 and (d) La/Z-S40. (C) Raman spectra of (a) Z-S40, (b) La/Z-S40.

presence of deposited coke species.

Raman spectroscopy analysis is a unique technique for coke characterization. The type and nature of deposited coke over Z-S40 and La/Z-S40 samples are characterized, and the result is displayed in the Fig. 8(C). Various types of coked species are found to present in the samples. In the high frequency Raman region (1530–1660 cm⁻¹), an asymmetric and big peak with high intensity is observed for two samples, suggesting that various types of unsaturated carbonaceous species with similar Raman wavenumbers are presented. These Raman bands have been reported in literature. As described, the shoulder Raman bands at 1585–1595 cm⁻¹ and 1540–1560 cm⁻¹ are related to pre-graphitic particles [70,71]. The marked bands at 1605–1620 cm⁻¹ and 1620–1640 cm⁻¹ are attributed to the C=C stretching vibration in the polycyclic aromatics/aromatics species [70,72] and polyolefins/olefins [70,71], respectively, indicating that these carbonaceous species are the main components in the deposited coke over two samples. In the middle Raman region (1340–1480 cm⁻¹), the 1360–1390 cm⁻¹ band is associated with the breathing mode of the sp² sites only in the rings, not in the chains [73]. The small and broad band between 1440 and 1470 cm⁻¹ is assigned to the C–H bond vibrations due to the presence of olefins on the catalyst surface [70,74]. In the low frequency Raman region (1150–1250 cm⁻¹), the broad band at 1200–1220 cm⁻¹ is characteristic of C–H bond vibrations, which is an indicative of aliphatic compounds [65]. The band at 1180–1190 cm⁻¹ is generally attributed to the very poorly organized carbonaceous species, while its confirmation is still a matter of some dispute [73]. Those Raman data are in well agreement with the FTIR results. Two characterization results generally indicate that in the whole reaction progress, the

deposited coke in the decomposition of CH₃SH over two samples are largely composed of polycyclic aromatics, polyolefins, and pregraphitic particles, with a high fraction of long branched aliphatics and a larger amount of –CH and –CH₂ groups than –CH₃ groups. No difference in the type of deposited coke is found between those two samples. Compared to parent ZSM-5, La doped HZSM-5 has a better resistance to all those coke deposited species during the decomposition of CH₃SH.

It is known that the deactivation of ZSM-5-type catalysts is largely improved in this work by the incorporation of La species. The improvement of the deactivation of HZSM-5 during the catalytic decomposition of CH₃SH using La species could be explained by two aspects, i.e., the pre-inhibition of the formation of coke and the post-elimination of the formed coke. On the one hand, the decrease of the acid strength to suppress the formation of coke can be realized by occupying the strong Brønsted acid sites via the addition of La species. NH₃-TPD as shown in Fig. 9A is used to prove the original effect of La species on the strength of acid sites. The corresponding amount of acid sites is compiled in Table 2. As displayed in Fig. 9A, Z-F catalyst exhibits the typical NH₃-TPD profile with two maximum peaks at low and high temperature. The low temperature desorption peak at 270 °C has been assigned to the desorption of NH₃ from weak acid sites (such extra-framework aluminum) [75,76], while the high temperature desorption peak at 490 °C has been attributed to the desorption of NH₃ from the Brønsted acid sites deriving from framework aluminum [77,78]. When La species is doped into HZSM-5, the amount and strength of all the weak and strong acid sites decrease to different degree (from 474.44 and 234.87 μmol/g to 343.94 and 106.41 μmol/g, respectively). The significant decrease in the amount of strong acid sites may be owing to the

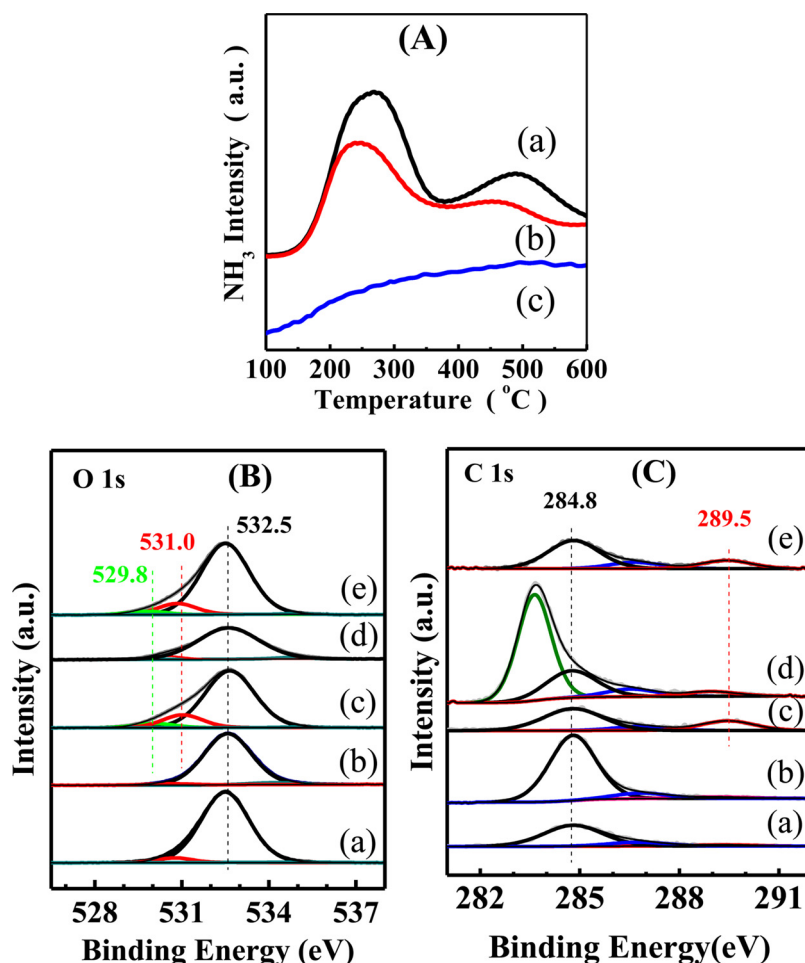


Fig. 9. (A) NH_3 -TPD profile of fresh samples: (a) Z-F, (b) La/Z-F and (c) Z-S40. Decomposition of XPS O 1 s (B) and C 1 s (C) spectra of the catalytic systems: (a) Z-F, (b) Z-S40, (c) La/Z-F, (d) La/Z-S40 and (e) La/Z-R1.

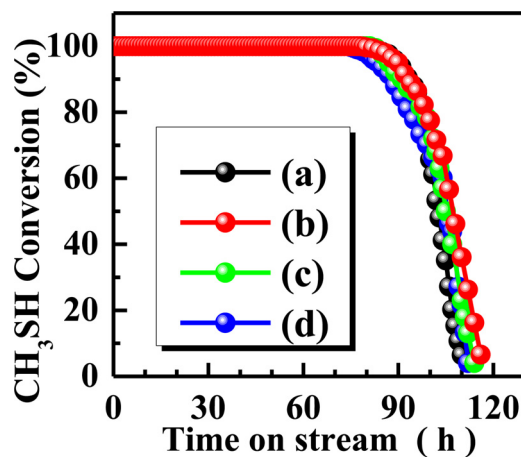


Fig. 10. The conversion of CH₃SH as a function of reaction time over (a) La/Z-F, (b) La/Z-R1, (c) La/Z-R2 and (d) La/Z-R3.

substitution of bridging Al-OH groups by the basic La-OH species because of the dealumination, as confirmed by the FT-IR spectrum (Fig. 2). It was well-documented that the stronger acidic strength together with the higher acid site concentration (or density) were in favor of the rapid deactivation of catalyst due to the acceleration of the coking rate [79,80]. The deactivation of zeolite-based catalysts is thus inevitable in many catalytic reactions (such as hydrocarbon cracking and methanol-to-hydrocarbons) due to the formation of carbonaceous

deposits on the strong acid sites [12,3,81,82]. In this work, decreasing the amounts of partially strong acid sites occupied by the addition of La species can inhibit the formation of coke at the source and should be beneficial to the significant improvement in their catalytic stability. Moreover, it should be noted that, although the amount of extra-framework aluminum increases, the amount of weak acid sites slightly decreases instead, which might be due to the interaction between the extra-framework Al (Lewis acid) and deposited basic La oxide species. Interestingly, in spite of the significant decrease in the amount of weak and strong acidic concentration with the incorporation of La into ZSM-5, the corresponding catalytic performance for La/Z-F catalyst greatly improved rather than declined at 400 $^{\circ}\text{C}$, especially 450 $^{\circ}\text{C}$ (Fig. 1). This suggests that a certain fraction of the active acidic sites still remain accessible for the reactant molecules, CH₃SH, as well as, importantly, some new active sites are available, as confirmed before.

The coke deposited on the catalyst surface, on the other hand, would be gradually eliminated after the coke were formed. The previous results indicate that the enhanced catalytic activity of CH₃SH decomposition over La/Z-F sample is closely related to the presence of surface active oxygen species, which can react with carbon containing reactants to produce CO₂ gas. Hence, the produced CO₂ could act as a scavenger to remove the deposited coke to some degree [83,84], as shown by Eq. (1), which is one of the main factors increasing the stability of La/Z-F sample. However, it is not clear that if there are any direct contributions of those surface lattice oxygen species, especially, carbonated oxygen from La₂O_x(CO₃)_y to eliminate the coke deposited for the long term stability of La/Z-F sample. Therefore, the XPS O 1 s and C 1 s spectra of Z-F, La/Z-F, Z-S40, La/Z-S40, and La/Z-R1 samples

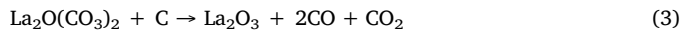
Table 3

The binding energy and surface element composition for Z-F, La/Z-F, Z-S40, La/Z-S40, and La/Z-R1 samples.

Catalyst	Relative content of oxygen and carbon (%) ^a		
	Lattice Oxygen	Oxygen from $\text{CO}_3^{2-}/\text{OH}^-$	Carbon from CO_3^{2-}
Z-F	0	4.7 (530.9)	6.4 (289.1)
Z-S40	0	2.0 (530.6)	22.7 (289.1)
La/Z-F	4.9 (529.8)	15.1 (531.0)	41.5 (289.6)
La/Z-S40	0.2 (529.6)	3.3 (530.5)	19.4 (289.5)
La/Z-R1	4.0 (529.9)	13.0 (530.9)	32.5 (289.5)

^a The relative content of oxygen and carbon species were calculated according to oxygen species at 532.5 eV in the O1 s spectra and to adventitious carbon at 284.8 eV in the C1 s spectra, respectively.

are shown in Fig. 9(B) and (C), respectively, to explain the role of surface oxygen species on the deposited coke. The corresponding binding energy and relative content of oxygen species are compiled in Table 3. As shown by Fig. 9(B) and Table 3, in the La/Z-F sample, three kinds of main oxygen species, surface lattice oxygen, surface carbonated oxygen from $\text{CO}_3^{2-}/\text{OH}^-$, and oxygen from framework Si-O-Si groups, are presented, as evidenced by the previous XPS results. Compared to the fresh Z-F and La/Z-F samples, after the stability test of 40 h, the relative contents of all the surface lattice oxygen and carbonated oxygen species of Z-S40 and La/Z-S40 samples largely decrease from 4.9% and 15.1% to 0.2% and 3.3%, respectively, indicating that the active oxygen species are consumed during the stability test. When the spent La doped ZSM-5 sample was regenerated once, the relative contents of the surface lattice oxygen and surface carbonated oxygen species in La/Z-R1 sample return to the original value (from 0.2% and 3.3% for La/Z-S40 to 4.0% and 13% for La/Z-R1 sample, respectively). It is accepted that the interaction of surface lattice oxygen and surface carbonated oxygen from $\text{La}_2\text{O}_x(\text{CO}_3)_y$ with deposited coke could decrease the relative contents of reactive oxygen species on the catalysts surface, generating the gas products, CO_2 and CO, as described by Eqs. (1) and (2), and resisting the deactivation of La doped ZSM catalyst. The variation in the relative contents of CO_3^{2-} species also demonstrates this result. Fig. 9C (c) shows that the binding energy at 289.5 eV of La/Z-F sample is attributed to the presence of CO_3^{2-} species. After reaction of 40 h, the CO_3^{2-} species are consumed and the corresponding relative content decreased from 41.5% to 19.4%. With the regeneration proceeded, the relative content of CO_3^{2-} species of La/Z-R1 sample again recover from 19.4% to 32.5%, suggesting the participation of CO_3^{2-} species into the process of eliminating the deposited coke. These results demonstrate that deposited coke species well react with the active oxygen species in the $\text{La}_2\text{O}_x(\text{CO}_3)_y$ species. In fact, there is a possibility of the equilibrium of chemisorption and dissociation between La_2O_3 and CO_2 during the reaction process at an expense of surface active oxygen species. Some studies reported that the generation of $\text{La}_2\text{O}_x(\text{CO}_3)_y$ species was in favor of eliminating the deposited coke around the active center, retarding the deactivation in some catalytic reactions, including carbon dioxide reforming of methane [85], and catalytic combustion of diesel soot [24].



Moreover, one distinct peak at 283.8 eV is observed for La/Z-S40 sample (Fig. 9C (d)). Compared to the binding energy of contaminated carbon at 284.8 eV, the value of binding energy is shifted to low position by 1.0 eV. According to the literature, a low binding energy at 283.8 eV has been ascribed to the carbon in ethylene species chemisorbed on the rhodium [86], platinum [87], and iridium [88] species. In this study, since La species could act as additional active sites, the coke

in the form of polyolefins generated during the stability test is possible to be chemisorbed on the La species, which could form the carbon species with low binding energy at 283.8 eV. However, this phenomenon could not be proved, because of the lack of in-situ characterization of this species. The formation of La-C mixed structure or some other foreign carbon species cannot be excluded.

Combining the results of CO_2 -TPD, NH_3 -TPD, XPS, and FT-IR with the CH_3SH -TPD analyses, the roles of La for enhancing the catalytic activity and stability can be explained as follows. For HZSM-5 catalyst, CH_3SH molecule could be easily absorbed on the basic sites of the catalyst because of its acidic characteristic and then be migrated to the acidic active sites for the enhanced decomposition of CH_3SH [5,14,15], as also confirmed by the NH_3 -TPD of the coked HZSM-5 (Fig. 9A (c)) as well as the stability result of HZSM-5 (Fig. 6). With the addition of La, an additional basic active sites is generated, which promotes the CH_3SH molecule to be adsorbed, activated, and reacted due to the increase in the basic sites accompanied by the basicity strength. Furthermore, as for stability, the decrease in the amount (or concentration) of strong acid sites via the addition of La species retards the formation rate of coke deposits. The large amounts of CO_2 produced over La/Z-F catalyst can offer an oxidizing character to destabilize and eliminate the carbonaceous deposits around the acid active sites during the decomposition of CH_3SH , which provides a direct proof to demonstrate that the modification of La is conducive to improve the catalytic stability of La/HZSM-5. Moreover, the coke deposits on the catalysts surface would be easily oxidized and eliminated due to the effect of the produced surface $\text{La}_2\text{O}_x(\text{CO}_3)_y$ species.

3.5. Catalyst regeneration

For the purpose of industrial application, catalyst regeneration was carried out to investigate whether the spent La-doped HZSM-5 catalyst can be effectively regenerated or not and the catalytic stability of the regenerated La/HZSM-5 catalyst. The corresponding results are exhibited in Fig. 10. To our surprise, spent La-doped HZSM-5 catalyst can be well recovered to its original stability after regeneration. More importantly, even after three cycles of deactivation-regeneration, the catalytic stability of the regenerated La-doped HZSM-5 catalyst is comparable to that of fresh La/HZSM-5 catalyst. Based these results of catalyst regeneration, it is concluded that La-doped HZSM-5 is an efficient catalyst for CH_3SH elimination.

4. Conclusion

In summary, La-doped HZSM-5 catalyst exhibited higher catalytic activity and longer term stability than those of parent HZSM-5 catalysts. Especially, La doped HZSM-5 catalyst exhibited excellent stability without significant deactivation even after 90 h TOS test, whereas parent HZSM-5 was rapidly deactivated within 18 h under the same reaction conditions. The enhanced catalytic performances of La doped HZSM-5 catalysts were closely associated with their tunable acid-base properties, surface reactive oxygen species and the generated CO_2 and surface lanthanum oxy-carbonates. On the one hand, the generation of basic sites within the La-doped HZSM-5 catalysts would be in favor of the adsorption, activation and reaction of intermediate and reactant molecules. More importantly, the surface reactive and available oxygen species in La species can be provided as additional active sites to react with carbon containing molecule to generate CO_2 , improving the catalytic activity of decomposing CH_3SH . On the other hand, the decrease in the amount of strong acid sites of the La-doped HZSM-5 catalysts with respect to parent HZSM-5 would effectively suppress the formation of coke deposit within the catalysts. The produced CO_2 and surface generated lanthanum oxy-carbonates could also effectively eliminate the deposited coke in the form of polyaromatics and polyolefins, branched aliphatics and $-\text{CH}_2$, $-\text{CH}_2$ groups and $-\text{CH}_3$ groups. The spent La doped HZSM-5 catalyst can be effectively regenerated for many

times via a facile and rapid method, and no significant deactivation was found after three cycles of deactivation-regeneration, indicating that La doped HZSM-5 was an excellent catalyst for catalytic decomposition of CH₃SH.

Acknowledgements

The National Natural Science Foundation of China (U1402233, 21667016 and 21267011) and Young Academic and Technical Leader Raising Foundation of Yunnan Province (2008py010) are gratefully acknowledged for the financial support for this research work.

References

- [1] R. Zhang, A. Khalizov, L. Wang, M. Hu, W. Xu, *Chem. Rev.* 112 (2012) 1957–2011.
- [2] S. Guo, M. Hua, M. Zamora, J. Peng, D. Shang, J. Zhang, Z. Du, Z. Wu, M. Shao, L. Zeng, M. Molina, R. Zhang, *PNAS* 111 (2014) 17373–17378.
- [3] M. Stephanopoulos, M. Sakbodin, Z. Wang, *Science* 312 (2006) 1508–1510.
- [4] M. Behl, J. Yeom, Q. Lineberry, P. Jain, M. Shannon, *Nat. Nanotechnol.* 7 (2012) 810–815.
- [5] D. He, D. Chen, H. Hao, J. Yu, J. Liu, J. Lu, F. Liu, G. Wan, S. He, Y. Luo, *Appl. Surf. Sci.* 390 (2016) 959–967.
- [6] N. Laosiripojana, S. Assabumrungrat, *Appl. Catal. B-Environ.* 102 (1) (2011) 267–275.
- [7] K.M. Brown, W.K.T. Gleim, P. Urban, *Oil Gas J.* 57 (1959) 73–78.
- [8] P. Briot, R. Cadours, S. Drozdz, F. Lecomte, US Patent 2007/0193925.
- [9] A. Carlsson, G. J. Heeringen, US Patent 2009/00447201.
- [10] E. Huguet, B. Coq, R. Durand, C. Leroi, R. Cadours, V. Hulea, *Appl. Catal. B-Environ.* 134–135 (2013) 344–348.
- [11] H. Vasile, H. Edouard, C. Claudia, L. Antoine, D. Robert, L. Catherine, C. Renaud, C. Bernard, *Appl. Catal. B-Environ.* 156 (2014) 128–133.
- [12] D. He, G. Wan, H. Hao, D. Chen, J. Lu, L. Zhang, F. Liu, L. Zhong, S. He, Y. Luo, *Chem. Eng. J.* 289 (2016) 161–169.
- [13] D. He, H. Hao, D. Chen, J. Liu, J. Yu, J. Lu, F. Liu, G. Wan, S. He, Y. Luo, *Catal. Today* 281 (2017) 559–565.
- [14] D. He, H. Hao, D. Chen, J. Liu, J. Yu, J. Lu, F. Liu, S. He, K. Li, Y. Luo, *Appl. Catal. A: Gen.* 533 (2017) 66–74.
- [15] D. He, D. Chen, H. Hao, J. Yu, J. Liu, J. Lu, G. Wan, S. He, K. Li, Y. Luo, *Chem. Eng. J.* 317 (2017) 60–69.
- [16] K.A. Tarach, J. Martinez-Triguero, F. Rey, K. Góra-Marek, *J. Catal.* 339 (2016) 256–269.
- [17] M.R. Sáez, D. Divakar, A. Aranzabal, J.R.G. Velasco, J.A.G. Marcos, *Appl. Catal. B-Environ.* 180 (2016) 210–218.
- [18] V. Hulea, E. Huguet, C. Cammarano, A. Lacarriere, R. Durand, C. Leroi, R. Cadours, B. Coq, *Appl. Catal. B-Environ.* 144 (2014) 547–553.
- [19] S. Campbell, D. Bibby, J. Coddington, R. Howe, R. Meinhold, *J. Catal.* 161 (1996) 338–349.
- [20] P. Losch, A.B. Pinar, M.G. Willinger, K. Soukup, S. Chavan, B. Vincent, P. Pale, B. Louis, *J. Catal.* 345 (2017) 11–23.
- [21] K. Wakui, K. Satoh, G. Sawada, *Catal. Lett.* 81 (1–2) (2002) 83–88.
- [22] J.C. Lu, X.F. Li, S.F. He, C.Y. Han, G.P. Wan, Y.Q. Lei, R. Chen, P. Liu, K.Z. Chen, L. Zhang, Y.M. Luo, *Int. J. Hydrogen Energy* 42 (2017) 3647–3657.
- [23] C.V. Ramana, R.S. Vemuri, V.V. Kaichev, V.A. Kochubey, A.A. Saraev, V.V. Atuchin, *ACS Appl. Mater. Interfaces* 3 (2011) 4370–4373.
- [24] J.M. Moggia, V.G. Milt, M.A. Ulla, L.M. Cornaglia, *Surf. Interface Anal.* 35 (2003) 216–225.
- [25] B.S. Liu, L. Jiang, H. Sun, C.T. Au, *Appl. Surf. Sci.* 253 (2007) 5092–5100.
- [26] R. Borade, A. Sayari, A. Adnot, S. Kaliaguine, *J. Phys. Chem.* 94 (1990) 5989–5994.
- [27] C. Han, H. Li, H. Pu, H. Yu, L. Deng, S. Huang, Y. Luo, *Chem. Eng. J.* 217 (2013) 1–9.
- [28] C. Han, H. Pu, H. Li, L. Deng, S. Huang, S. He, Y. Luo, *J. Hazard. Mater.* 254–255 (2013) 301–309.
- [29] Y. Han, J. Ying, *Angew. Chem. Int. Ed. Engl.* 44 (2005) 288.
- [30] L. Zhang, C. Han, H. Wang, H. Pu, D. Du, J. Li, Y. Luo, *Mater. Res. Bull.* 47 (2012) 3931–3936.
- [31] B. Puértolas, L.G. Andújar, T. García, M.V. Navarro, S. Mitchell, J.P. Ramírez, *Appl. Catal. B-Environ.* 154–155 (2014) 161–170.
- [32] K. Barbera, F. Bonino, S. Bordiga, T.V.W. Janssens, P. Beato, *J. Catal.* 280 (2011) 196–205.
- [33] G. Yang, Y. Wang, D. Zhou, J. Zhuang, X. Liu, X. Han, X. Bao, *J. Chem. Phys.* 119 (2003) 9765.
- [34] H. Matsuura, N. Katada, M. Niwa, *Microporous Mesoporous Mater.* 66 (2003) 283–296.
- [35] K.G. Marek, K. Brylewskas, K.A. Tarach, M. Rutkowska, M. Jabłońska, M. Choi, L. Chmielarz, *Appl. Catal. B-Environ.* 179 (2015) 589–598.
- [36] P. Tynjäkkö, T.T. Pakkanen, *J. Mol. Catal. A: Chem.* 110 (1996) 153–161.
- [37] V.G. Milt, R. Spretz, M.A. Ulla, E.A. Lombardo, *Catal. Lett.* 42 (1996) 57–63.
- [38] N. Topsoe, K. Pedersen, E.G. Derouane, *J. Catal.* 70 (1981) 141.
- [39] I. Othman, R.M. Mohamed, I.A. Ibrahim, M.M. Mohamed, *Appl. Catal. A: Gen.* 299 (2006) 95–102.
- [40] J.I. Villegas, N. Kumar, T. Salmi, D.Yu. Murzin, T. Heikkila, P. Hudec, A. Smieskova, *Stud. Surf. Sci. Catal.* 158 (2005) 1859–1866.
- [41] P. Szama, B. Wichterlova, J. Dedecek, Z. Tvaruzkova, Z. Musilova, L. Palumbo, S. Sklenak, O. Gonsiorova, *Microporous Mesoporous Mater.* 143 (2011) 87–96.
- [42] Y.M. Luo, Z.Y. Hou, D.F. Jin, X.M. Zheng, *Chin. J. Chem.* 25 (2007) 635–639.
- [43] L. Wang, H. Chen, M.H. Yuan, S. Rivillon, E.H. Klingenberg, J.X.M. Li, R.T. Yang, *Appl. Catal. B-Environ.* 152–153 (2014) 162–171.
- [44] S. Hamid, M.A. Kumar, W. Lee, *Appl. Catal. B-Environ.* 187 (2016) 37–46.
- [45] A. Cihanoglu, G. Gündüz, M. Dükkancı, *Appl. Catal. B-Environ.* 165 (2015) 687–699.
- [46] C. Han, H. Wang, Li.R. Zhang, Y. Zhang, Y. Luo, X. Zheng, *Adv. Powder Technol.* 22 (2011) 20–25.
- [47] H. Pu, C. Han, H. Wang, S. Xu, L. Zhang, Y. Zhang, Y. Luo, *Appl. Surf. Sci.* 258 (2012) 8895–8901.
- [48] H.Y. Chen, L. Chen, J. Lin, K.L. Tan, *Inorg. Chem.* 36 (1997) 1417–1423.
- [49] G. Coudrier, C. Naccache, J.C. Vedrine, *J. Chem. Soc. Chem. Commun.* (1982) 1413.
- [50] V.G. Milt, R. Spretz, M.A. Ulla, E.A. Lombardo, J.L.G. Fierro, *Catal. Lett.* 42 (1996) 57.
- [51] A.J. Nelson, T. van Buuren, T.M. Willey, C. Bostedt, J.J. Adams, K.I. Schaffers, L. Terminello, T.A. Callcott, *J. Electron. Spectrosc.* 137–140 (2004) 541–546.
- [52] B.M. Reddy, B. Chowdhury, P.G. Smirniotis, *Appl. Catal. A: Gen.* 219 (2001) 53–60.
- [53] E.S. Shpiro, W. Griniert, R.W. Joyner, G.N. Baeva, *Catal. Lett.* 24 (1994) 159–169.
- [54] J.L. Hueso, A. Caballero, M. Ocaña, A.R. González-Elipe, *J. Catal.* 257 (2008) 334–344.
- [55] G.R. Gallaher, J.G. Goodwin, C.S. Huang, M. Houalla, *J. Catal.* 140 (1993) 453–463.
- [56] S. Ponce, M.A. Peña, J.L.G. Fierro, *Appl. Catal. B-Environ.* 24 (2000) 193–205.
- [57] P.A.W. van der Heide, *Surf. Interface Anal.* 33 (2002) 414–425.
- [58] P. Castaño, A. Gutierrez, I. Hita, J.M. Arandes, A.T. Aguayo, J. Bilbao, *Energy Fuels* 26 (2012) 1509–1519.
- [59] D. Chen, D. He, J. Lu, L. Zhong, F. Liu, J. Liu, J. Yu, G. Wan, S. He, Y. Luo, *Appl. Catal. B-Environ.* 218 (2017) 249–259.
- [60] M. Yang, S. Li, G. Chen, *Appl. Catal. B-Environ.* 101 (2011) 409–416.
- [61] C. Liu, L. Chen, J. Li, L. Ma, H. Arandiany, Y. Du, J. Xu, J. Hao, *Environ. Sci. Technol.* 46 (2012) 6182–6189.
- [62] D. Brion, *Appl. Surf. Sci.* 5 (1980) 133.
- [63] B.J. Lindberg, K. Hamrin, G. Johansson, U. Gelius, A. Fahlmann, C. Nordling, K. Siegbahn, *J. Phys. Scripta* 1 (1970) 286.
- [64] J.A.T. Antonio, M.A.C. Jacome, C.A. Chavez, J. Escobar, M.C. Barrera, E.L. Salinas, *Appl. Catal. B-Environ.* 90 (2009) 213–223.
- [65] A.T. Aguayo, P. Castaño, D. Mier, A.G. Gayubo, M. Olazar, J. Bilbao, *Ind. Eng. Chem. Res.* 50 (2011) 9980–9988.
- [66] M. Rutkowska, D. Macina, N. Miroscha-Kubien, Z. Piwowarska, L. Chmielarz, *Appl. Catal. B-Environ.* 174–175 (2015) 336–343.
- [67] L. Palumbo, F. Bonino, P. Beato, M. Bjørgen, A. Zecchina, S. Bordiga, *J. Phys. Chem. C* 112 (2008) 9710–9716.
- [68] S. Kim, E. Sasmaz, J. Lauterbach, *Appl. Catal. B-Environ.* 168–169 (2015) 212–219.
- [69] M. Rozwadowski, M. Lezanska, J. Włoch, K. Erdmann, R. Golembiewski, J. Kornatowski, *Chem. Mater.* 13 (2001) 1609–1616.
- [70] C. Li, P.C. Stair, *Catal. Today* 33 (1997) 353–360.
- [71] S. Kubá, H. Knozinger, J. Raman Spectrosc. 33 (2002) 325–332.
- [72] L. Lin, W. Lin, Y.X. Zhu, B.Y. Zhao, Y.C. Xie, *Langmuir* 21 (2005) 5040–5046.
- [73] J.A. Botas, D.P. Serrano, A. García, J. de Vicente, R. Ramos, *Catal. Today* 195 (2012) 59–70.
- [74] P.E. Eberly Jr, *J. Phys. Chem.* 71 (1967) 1717–1722.
- [75] N. Katada, H. Igai, J. Kim, M. Niwa, *J. Phys. Chem. B* 110 (1997) 5969–5997.
- [76] L.R. González, F. Hermes, M. Bertmer, E.R. Castellón, A.J. López, U. Simon, *Appl. Catal. A: Gen.* 328 (2007) 174–182.
- [77] J.C. Groen, L.A.A. Peffer, J.A. Moulijn, J. Pérez-Ramírez, *Chem. Eur. J.* 11 (2005) 4983–4994.
- [78] L. Lin, C. Qiu, Z. Zhuo, D. Zhang, S. Zhao, H. Wu, Y. Liu, M. He, *J. Catal.* 309 (2014) 136–145.
- [79] J.F. Haw, W. Song, D.M. Marcus, J.B. Nicholas, *Acc. Chem. Res.* 36 (2003) 317.
- [80] U. Olsbye, S. Svelle, M. Bjørgen, P. Beato, T.V.W. Janssens, F. Joensen, S. Bordiga, K.P. Lillerud, *Angew. Chem. Int. Ed.* 51 (2012) 5810.
- [81] D. Mores, E. Stavitski, M.H.F. Kox, J. Kornatowski, U. Olsbye, B.M. Weckhuysen, *Chem. Eur. J.* 14 (2008) 11320.
- [82] M. Guisnet, L. Costa, F.R. Ribeiro, *J. Mol. Catal. A: Chem.* 305 (2009) 69–83.
- [83] X. Yu, N. Wang, W. Chu, M. Liu, *Chem. Eng. J.* 209 (2012) 623–632.
- [84] S.M. Lima, J.M. Assaf, *Catal. Lett.* 108 (2006) 63–70.
- [85] X. Yu, N. Wang, W. Chu, M. Liu, *Chem. Eng. J.* 209 (2012) 623–632.
- [86] R.J. Levis, L.A. De Louise, E.J. White, N. Winograd, *Surf. Sci.* 230 (1990) 35.
- [87] F. Zaera, *Surf. Sci.* 219 (1989) 453.
- [88] T.S. Marinova, K.L. Kostov, *Surf. Sci.* 181 (1987) 573.